PERGAMON

Aerosol Science 32 (2001) 509–524

Journal of
Aerosol Science

www.elsevier.com/locate/jaerosci

Observation of restructuring of nanoparticle soot aggregates in a diffusion flame by static light scattering

S. di Stasio*

Fluid Dynamics and Combustion Division, Istituto Motori-National Research Council of Italy, Via Marconi 8 - 80125 Napoli, Italy

Received 20 March 2000; accepted 27 July 2000

Abstract

Static light scattering experiments are performed within an ethylene–air diffusion flame for different flow-rates of the fuel gas. Direct evidence is here given about the fact that soot agglomerates, at the early stages of the agglomeration process, first grow as elongated chain-like structures and then, at later stages, assume more compact morphologies with significantly smaller size. This mechanism is observed to occur for the first time in a diffusion flame along the flame axis in the range of low heights-above-burner (HABs less than one fourth of the total flame length). Thus, branched elongated aggregates grow up at lower HABs to assume a radius of gyration $R_g \approx 380$ nm while the fractal dimension is practically constant $D_F^* \approx 1.3$. Thereafter, at larger HABs, they self-reorganise in much shorter clusters ($R_g \approx 160$ nm), with D_F^* increasing up to 1.9. Explanation is proposed for the observed rearrangement of soot fractal aggregates in terms of local heat transfer balance at cluster surface, which could cause, in the case of chain-like aggregates, a supplementary oxidation inside the pores of soot with possible breaking of the graphitic layers that act as bridges between primary particles within an aggregate. The relevance of depolarised scattered light is discussed with regard to some distinguishing features of clusters that share the same measured fractal dimension.

Keywords: Nanoparticle aggregates; Fractal-like structures; Polarised scattering; Flame; Soot

1. Introduction

Flames are often used to generate nanoparticle aggregates of soot (Sorensen & Feke, 1996; Köylü, Xing, & Rosner, 1995; Faeth & Köylü, 1995), titania (Rogak, Baltensperger, & Flagan,

* Corresponding author. Tel.: + + 39-081-71-77-122; fax: + + 39-081-239-60-97.
E-mail address: stefano@motori.im.na.cnr.it (S. di Stasio).

0021-8502/01/$ - see front matter
PII: S0021-8502(00)00098-7

1991) or silica (Hurd & Flower, 1988). The nature of such flame-generated materials is recognised to be fractal (Dobbins & Megaridis, 1991; Dobbins, Mulholland, & Bryner, 1994; Sorensen & Feke, 1996), even if, recently, some criticism about the concept of universality of fractal laws has been moved (Malcai, Lidar, Biham, & Avnir, 1997). As a matter of fact, it is well-known that fractal analysis and self-similarity concepts are valid within particular inspection scales (Freltoft, Kjems, & Sinha, 1986) for which a power law exists between the scaling of cluster mass and size. Scaling and power density correlation hold true within a range of lengths that extends from the mean size a_P of primary sub-units constituting fractal clusters (lower cut-off) to a length ξ (upper cut-off) known as the *correlation length* of the aggregates (Bunde & Havlin, 1994,1996). Within this range, the fractal approach is a valuable tool to classify complex assemblies of nanoparticle sub-units. Soot particles in flames are nucleated at lower heights above the burner in correspondence of residence times of about 1 ms. Following the stream of the hot gas they undergo a fast surface growth process, and, contemporarily, they are subjected to collision and sticking mechanisms with formation of aggregates. Particle dynamics is governed by the strong Brownian motion and by the attractive short-range van der Walls forces. Generally speaking, the physical appearance of flame generated soot is of wispy, branched structures composed by spheroid sub-units, called *monomers* or primary *spherules*, with dimensions a_P narrowly confined in the range 10–50 nm, depending on flame type and fuel nature, with a typical log-normal size distribution (Megaridis & Dobbins, 1989; Faeth & Köylü, 1995; Köylü, 1996). Single-flame agglomerates are usually 100–700 nm in maximum length and are constituted by some hundreds of monomers (Faeth & Köylü, 1995). Diffusion-limited cluster–cluster aggregation (DL-CCA) is usually considered to apply to soot cluster agglomeration kinetics (Oh & Sorensen, 1997). The universally accepted value of fractal dimension obtained for 3-D DL-CCA computer simulations is 1.8 (Asnaghi, Carpineti, Giglio, & Sozzi, 1992), independent of the nature of the nanoparticles involved in the aggregation process. Electric charge and ionisation state have been reported in the past to play a significant role in determining the structure of soot clusters in flames (Howard, 1969; Wersborg, Howard, & Williams, 1973). Charge effects, probably, contribute to determine the lower value of fractal dimension reported in the experiments with respect to the computational results (Onischuk et al., 2000a, b).

One of the most interesting challenges of nanoparticle aerosol research nowadays is to understand and predict the collective behaviour of ensemble of such particles in relation to the local thermal and mechanical interactions as heat transmission (Chen, 1996), elastic behaviour (Friedlander, Jang, & Ryu, 1998), neighbouring shell interactions (Dimon et al., 1986), global reorganisation (Weber & Friedlander, 1997a). This is not a trivial issue to be pursued, especially in hostile environments, such as it is a flame where transformation of chemical species takes place at very high temperatures and on very short time scales.

Scattering techniques are very powerful tools (Martin & Hurd, 1987; Kjems, 1996) to infer in situ the structural parameters of fractal aggregates in harsh environment. Main advantages of such diagnostics are the facts that no sampling is required, and that no a priori knowledge of the refractive index of the investigated material is strictly necessary. Specifically, static scattering experiments measure the spatial fluctuations in the scattering length density, which, depending on the nature of the probing beam, namely, laser light, X-rays, neutrons, is the effect of the refractive index variations, electron density and nuclear scattering lengths, respectively (Kjems, 1996). Light scattering techniques, which obtain the angular patterns of co-polarised scattered light, i.e., the light scattered with the same (vertical) linear polarisation state of incident light, have been

extensively applied to soot aggregates in flames to recognise the fractal dimension and the radius of gyration (Dobbins & Megaridis, 1991; Sorensen, Cai, & Lu, 1992).

The structure of nanoparticle agglomerates of different nature, such as Ag, NaCl or soot has been investigated both in coagulation chambers (Kütz & Schmidt-Ott, 1993) and in the atmosphere (Burtscher, Leonardi, Steiner, Baltensperger, & Weber, 1993) in the past years.

The mechanical properties of fractal aggregates have been also investigated. Some consideration about the stretching and bonding of fractal aggregates has been reported by Feng (1985) and Webman and Grest (1985). Early studies about the mechanism of restructuring for silver aggregates were authored by Schmidt-Ott (1988a). Restructuring of single very large (~ 10 μm) carbonaceous agglomerates is reported (Nyeki & Colbeck, 1995) to occur inside a modified Millikan cell as effect of bias reversing of a DC electric field. Some theoretical predictions about the effect of structure collapsing by fractal aggregates beyond a critical size has been formulated on the basis of divergence of density of states at low frequencies (Webman & Grest, 1985). More recent contributions on silver and copper nanoparticle chain aggregates (Weber and Friedlander, 1997b) have shown that this process is favoured by the higher temperatures, at which the measured energy of activation for restructuring is much smaller with respect to the energy of detachment (evaporation) for a single particle from the aggregate.

The aim of this paper is to report the first, to our knowledge, direct on-line experimental evidence in a diffusion flame about the occurring of spatial reorganisation of soot nanoparticle aggregates. In particular, the existence of a net restructuring of nanoparticle aggregates is here directly observed in an ethylene–air flame (flux rates of cold gaseous fuel about 11 cm^3s^{-1}) at HABs along flame axis lower than one-fourth of the total flame length $L_{flame} \approx 17$ cm. Thus, soot aggregates are found in the experiments, first, to grow within the flame as branched chains with increasing length and D_F^* about 1.2. At longer residence times, they pass the condition corresponding to $R_g \approx 330$ nm, $D_F^* \approx 1.3$) and, thereafter, they undergo a spatial reorganisation that leads to the formation of more dense and compact structures that correspond to much smaller R_g and larger D_F^*. No evidence of significant sintering process between soot aggregates is observed by scanning electron microscopy (resolution about 3 nm) at the heights-above-burner considered in this study.

2. Theoretical features

Mass (M) fractal-like objects are characterised in terms of the empirical law $M \propto (2R_g/a_P)^{D_F^*}$, which is considered to hold true in a statistical (not necessarily mathematical) sense. In the previous equation R_g and a_P are the aggregate gyration radius and the primary size and the notation D_F^* accounts for the limit of validity of the fractal law with respect to the universal case (power exponent D_F). In the case of constant primary particle mass, the proportionality factor k_F between fractal mass and $R_g^{D_F^*}$, that is known as *pre-factor* or *structural coefficient*, depends on the interactions between each primary particle within the aggregate and its nearest-neighbour particles. Pre-factor k_F, in turn, can be put into relationship with the so-called co-ordination number c_N (Weber & Friedlander, 1997a).

A similar relationship written as $M \propto (D_m/a_P)^{D_F^*}$ where D_m and a_P are the mobility equivalent diameter of the aggregate and the primary diameter, respectively, was first introduced and applied by Schmidt-Ott (1988b) and Schmidt-Ott, Baltensperger, Gäggeler, and Jost (1990) to determine

the fractal dimension from the measurements of mobility diameter and a quantity proportional to the aggregate mass. Considerable contribution is reported by Kasper (1982) about the mutual relationships between the concepts of mobility, aerodynamic and volume equivalent diameters for non-spherical particles characterised by different shape factors.

Fractal clusters are found to scatter light with particular phase fluctuation properties, which are physically determined by the spatial correlations existing in the structural assemblies of primary constituents of aggregated objects. Specifically, the measured intensity I^{A}_{VV} of light scattered with the same linear vertical polarisation of the incident light can be expressed as function of the modulus of the scattering vector (or momentum transfer) $q \equiv (4\pi/\lambda)\sin(\theta/2)$, as the following (Kjems, 1996):

$$I^{A}_{VV}(q) = (N/\upsilon)P(q)S(q), \tag{1}$$

where $\rho \equiv N/\upsilon$ is the density of scatterers in the volume υ. The term $P(q)$ represents the scattering function for an uncorrelated ensemble of monomers and is known as the average *form factor*, and the term $S(q)$ accounts for the inter-monomer scattering contribution and is called the *structure factor*. Before the onset of agglomeration, the isolated non-interacting monomers do behave as Rayleigh particles, for which I_{VV} is independent from the polar scattering angle θ (Bohren & Huffman, 1983). Thus, the angular patterns of I^{A}_{VV} predicted for isolated Rayleigh particles are flat against the polar angle θ. Structure factor $S(q)$ can be interpreted as the Fourier transform of the spatial pair correlation function $g(\mathbf{r})$ (Martin & Hurd, 1987; Gangopadhyay, Elminyawi, & Sorensen, 1991). This, in turn, must contain as factor a *cut-off function* $h(\mathbf{r}/\xi)$ where ξ is the *correlation length* of the fractal aggregate.

In our experiments the fractal dimension and the radius of gyration are determined by the measured angular patterns of the scattered light I^{A}_{VV} in correspondence to two limiting scattering behaviours that correspond of the so-called *power law*, $q^2R_g^2 \gg 1$, and *Guiner regime*, $q^2R_g^2 \leqslant 1.5\ D_F^*$ (Dobbins, Santoro, & Semerjian, 1990). In this last case the normalised scattering intensity can be written as

$$I^{A}_{VV}(q)/I^{A}_{VV}(0) \approx \exp(1 - q^2R_g^2/3). \tag{2a}$$

The above equation is further approximated by the following (Dobbins & Megaridis, 1991) that is not depending on the D_F^* value

$$I^{A}_{VV}(q)/I^{A}_{VV}(0) \approx 1 - q^2R_g^2/3, \quad q^2R_g^2 \ll 1. \tag{2b}$$

Eq. (2b) is verified if the condition $q^2R_g^2 \leqslant 0.3$ is fulfilled. We will assume this criterion for the evaluation of the radius of gyration from scattering measurements at small θ angles.

In the power-law regime the scattering intensity is written as (Dobbins & Megaridis, 1991; Kjems, 1996)

$$I^{A}_{VV}(q) \approx q^{-D_F^*}, \quad q^2R_g^2 \gg 1. \tag{3}$$

D_F^* and R_g are found out by the best fit of experimental data (Dobbins & Megaridis, 1991) in the power law and Guiner and regimes, respectively. It is significant to specify that the Guiner and power approximation are valid independently from the particular cut-off (exponential, Gaussian, etc.) of pair correlation function, which, in turn, has effect on the shape of the transition regime between Guiner and power-law behaviours (Sorensen, Lu, & Cai, 1995).

Fractal scaling $I_{VV}^{A}(q) \approx q^{-D_F^*}$ is a property valid over a finite range of q (Freltoft et al., 1986). In particular, q must lie between about ξ^{-1} and a_P^{-1}. For q larger than a_P^{-1}, in the case of isotropic scatterers with smooth surfaces, the scattering behaviour corresponds to Porod's regime (Schmidt, 1991) that is described by the following equation:

$$I_{VV}^{A}(q) \propto q^{-4}, \quad qa_P > 1. \tag{4}$$

Cluster polydispersion is demonstrated from computer simulations (Thouy & Jullien, 1996) to yield scarce influence on the scattered intensity as far as the fractal dimension is less than two. Vice versa, the effects of the polydispersion have been found (Haw, Poon, & Pusey, 1997) to strongly influence the scattering patterns at high concentrations near the sol–gel transition.

3. Experimental set-up

The light scattering set-up is reported in Fig. 1. Soot aggregates are produced by a Bunsen burner (BB, inner diameter 10 mm) fuelled with ethylene (purity higher than 99%). To provide reproducibility of measurements the air inlet of the Bunsen burner is locked in such a way that a standard low (non-zero) air entrainment is produced in each experiment within the inner duct of the burner, where air and fuel mix flowing up the tube. Laser light source is an Argon Ion Laser (Ar^+), operating at line 514.5 nm with output power 350 mW (at power meter PWMT). The polarisation state of the emitted laser light is linear vertical. The laser light is modulated on-off by a programmable chopper (CHP) at 931 Hz. The detection system is composed of two lens L2, L3 (diameter 1 in., type plane-convex, focal length 300 and 50 mm, respectively), an interference filter

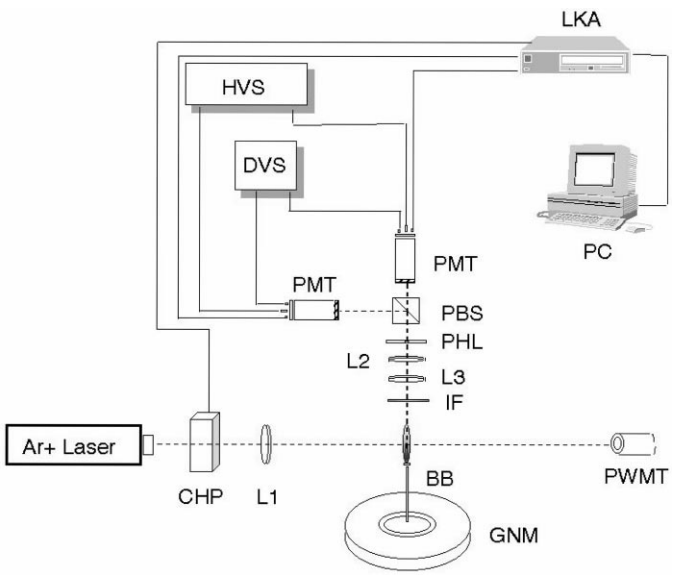

Fig. 1. Light scattering experimental set-up. Acronyms for each component are described in the text.

(IF) manufactured by Lot-Oriel (half-width spectral response equal to 1.043 nm), a pinhole (PHL) with diameter 1 mm, a polarising beam splitter (PBS) and two *side-on* photomultiplier tubes (PMTs) with preamplifier sockets. DVS and HVS represent dual voltage and high-voltage supply, respectively. The use of the interference filter allows the selective subtraction of the undesired contributions of blackbody emission and noise outside the band of detection. The measurement volume MV is determined in the experiments by the intersection of the laser beam and the optical detection cone (half-angle of detection 3.19°) and results about 40.7×10^{-6} mm^3 at 90°. At scattering angles θ different from 90° the probing volume MV results larger for a factor $1/\sin\theta$. Thus, the measured scattering signal at angle $\theta \neq 90°$ is normalised by multiplying the measurement times $\sin\theta$. In all measurements, a lock-in amplifier (LKA) is employed to provide the rejection of the noise out of the detection band.

The scattered light is split by the PBS into one contribution with the same linear polarisation state of the incident light, written as I_{VV}, and one other with polarisation orthogonal with respect to the incident light, I_{HV}. A number of 38 measurements at different polar angles in the range 15–160° are taken in a single experiment. In terms of the modulus q of the wave vector this corresponds to the range $2.0\ \mu m^{-1} < q < 24\ \mu m^{-1}$. Angular patterns of scattered light are measured at heights above burner (HABs) between 4 and 36 mm at radial co-ordinate zero (along the flame axis).

Measurements of monomer size within the same flame are reported in detail in a recent paper (di Stasio, 2000a). In particular, soot is collected on quartz disks exposed directly on the flame axis at different HABs. Nanoparticle aggregates impinge by thermophoresis effect on the support, thus producing immediate chemical quenching. Quartz samples with collected soot are thereafter subjected to a coating process, which produces the deposition of a chromium film (1.5 nm thickness) on their surface. Coating is obtained in vacuum conditions (10 μm Hg, equivalently ~ 1.3 Pa) obtained by a rotative pump Xenosput mod. XE 200. Thereafter, samples are positioned inside the test chamber of scanning electron microscope (SEM), where high-vacuum conditions are reproduced. The used SEM is of field emission type and it is manufactured by LEICA Cambridge 360 FE. The acceleration voltage used is typically 20 kV and the resolution about 3 nm for a probe current of 100 pA. A working example of micrograph obtained by SEM probing the flame on the axis at a HAB = 26 mm (cold ethylene flow rate about 7 cm^3 s^{-1}) is reported in Fig. 2. The primary average size as inferred in this case by SEM analysis on a set of about 50 aggregates from same quartz sample results 45 ± 7 nm. Some selected measurements of primary particle size a_P, for cold ethylene flow rate about 11 cm^3 s^{-1} are reported in Table 1. Thus, a_P is found to increase at HABs from 8 to 32 mm on the flame axis from about 16–43 nm, within an experimental uncertainty (one standard deviation of measurements) of about 15%. This is in accord with the finding of previous investigations (Megaridis & Dobbins, 1989) of similar diffusion flames at low HABs. At larger HABs the primary particle size is expected to increase up to a maximum size and thereafter to slightly decrease (Megaridis & Dobbins, 1989) as net effect of the balance between growth and oxidation rates.

Primary size is found to be weakly dependent on the cold-gas flow rate over the experienced range of flame total lengths (120–170 mm). More in particular, as reported elsewhere (di Stasio, 2000a), the primary particle sizes by SEM analysis, at parity of axial co-ordinate, are slightly smaller ($\approx -10\%$) for larger (11 cm^3 s^{-1}) with respect to smaller (7 cm^3 s^{-1}) ethylene flow rates.

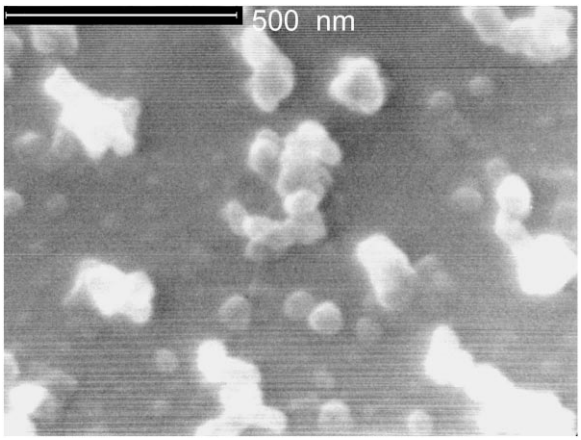

Fig. 2. Micrograph from scanning electron microscope of the soot particulate matter probed at 26 mm HAB in an ethylene–air diffusion flame. Acceleration voltage is 15 kV. The bar reported at bottom-left represents a scale of 500 nm. Cold-ethylene velocity at the entrance in the burner (inner diameter 10 mm) is 9.1 cm s^{-1} corresponding to a flow rate about 7 cm^3 s^{-1}. Bunsen burner is operated with the air-inlet blocked.

Table 1
Average size of primary particles from SEM analysis taken on ensembles of 50 aggregates from quartz probes inserted on the flame axis at different heights above the burner (HABs)[a]

HAB (mm)	$\langle a_P \rangle$ (nm)	σ (nm)
8	16	± 4
10	21	± 4
16	30	± 6
26	38	± 6

[a]Flow rate of cold ethylene fuelling the burner is about 11 cm^3 s^{-1}. We report in column 1 the HAB, in column 2 the corresponding primary average diameter and in column 3 the experimental error (one standard deviation) from measurements.

As a comment it is relevant to report that in the case of sampling at lower HABs, where smaller monomers are collected, the thermophoretic forces could drop with decreasing particle size thus producing an underestimation of the number of primary size in the smaller size classes of the relative primary size distribution. The net effect of such size-dependence of thermophoretic sampling could be an evaluation slightly in excess of the average primary dimension. It is worthwhile, however, to reflect that the investigation here reported about the dynamics of aggregate morphology as function of the residence times is essentially not influenced by the primary size that is very poorly changed within the investigated HABs.

The density of soot particles is obtained by helium pycnometry technique applied on soot collected at HAB = 60 mm on a metallic stagnation plate positioned inside the flame. A *stereo-pycnometer* manufactured by *Quantacrom* is used to measure the soot volume. The mass of the soot sample (about 200 mg) is obtained by weighting with an analytical balance. Soot density is

determined from the ratio of the two measurements. It is relevant to stress that the density inferred here is relative to the soot primary particles. Therefore, it is quite different from the apparent density of soot agglomerates that is lower with respect to the primary density. Helium is ordinarily chosen to perform pycnometry because helium molecule is characterised by a molecular size smaller with respect to other gas molecules, which favourites the penetration of the gas within the surface pore of soot. The estimation of the molecular diameter σ of the helium atom, obtained by the second virial coefficient B, is about 2.56 Å at 273 K and atmospheric pressure (Kaye & Laby, 1966). The limit of the above technique consists in the fact that some possibility exists that the helium molecule does not succeed to well penetrate the dendrite paths inside the soot structure, which are too narrow with respect to the helium molecular diameter σ. In this eventuality, the complete helium adsorption is not possible in all the soot volume. As a consequence of this, the measured soot volume could be estimated to be larger with respect to the true volume and the soot density, which is obtained as ratio of the soot weight and volume, could result smaller than the actual value. In our case, however, the soot density inferred by helium pycnometry technique is 2.0 g cm^{-3} that is in good accord with the data usually reported in the literature (see, for instance, Dobbins et al., 1994).

4. Results and discussion

Experiments are performed at two flow rates of the fuel gas, which determine different total length L_{flame} of the flame. At lower cold-gas efflux velocity ($v_{cold\text{-}gas} = 9.1$ cm s^{-1}, flow rate about 7 cm^3 s^{-1}, $L_{flame} \approx 120$ mm) a fractal dimension about 1.4 is found that is almost constant with respect to HAB, whereas the radius of gyration is slightly decreasing from about 237 ± 17 nm (HAB = 16 mm) to 202 ± 14 nm (HAB = 36 mm). At the larger ethylene flow rate ($v_{cold\text{-}gas} = 14.5$ cm s^{-1}, flow rate about 11 cm^3 s^{-1}, $L_{flame} \approx 170$ mm) a significant change of the fractal dimension is observed at different HABs.

Fig. 3 reports the angular pattern of the co-polarised scattered light intensity I_{VV} measured at HAB = 10 and 30 mm. The probing volume was centred on the flame axis. As already stated above, for isolated Rayleigh spherules the theoretical pattern of I^A_{VV} is flat against the scattering angle θ. Thus, the strong forward scattering lobe observed at 10 mm HAB is the evidence that the agglomeration process has already started at this axial co-ordinate with the formation of chain-like clusters. The enhancement of near-zero scattering over $I^A_{VV}(90^\circ)$ is about 10 at this stage. It should be reminded that angular scattering intensity near zero in the case of agglomerates composed by Rayleigh sub-units is enhanced with respect to the sum of the scattering intensities of the corresponding isolated Rayleigh particles by a factor proportional to the square of the mean number of primary particles per aggregate (di Stasio & Massoli, 1998). This is in general a property of the scattering by aggregates independent of their shape. A secondary peak of I^A_{VV} with respect to the forward main lobe is observed at angles about 120–140°. This peak is not expected from the theory of first-order Born approximation for small chain-like agglomerates (di Stasio & Massoli, 1997). The side lobe could be probably caused by the larger probing volume determined at angles other than 90° with the consequence of including different-sized primary particles and aggregates. It should be reported, in this regard, that in similar diffusion flames the primary size is not constant proceeding in radial direction from flame axis toward outside (Santoro, Smerjian, & Dobbins,

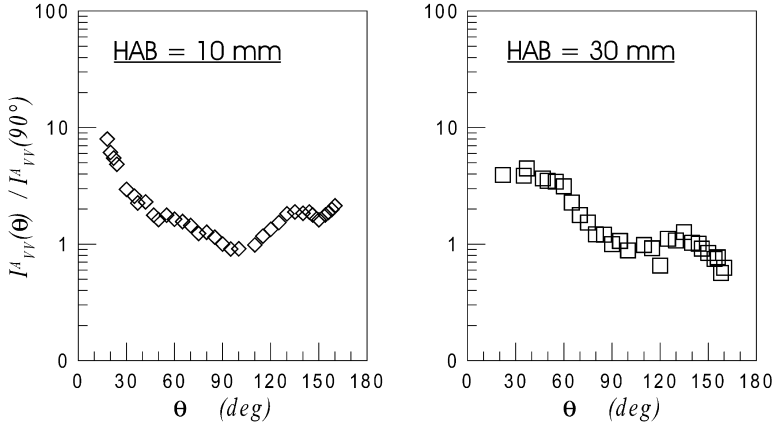

Fig. 3. Co-polarised scattered light I_{VV} vs. scattering angle θ in an ethylene–air diffusion flame ($L_{flame} \sim 170$ mm, $v_{cold-gas} = 14.5$ cm s^{-1}, flow rate is 11 cm^3 s^{-1}, air inlet of Bunsen burner is blocked). We report the angular patterns at 10 mm (left) and 30 mm (right) HAB. Radial co-ordinate with respect to flame axis is zero.

1983). Vice versa, at larger HAB = 30 mm (Fig. 3, right) the experimental evidence of a side peak at about 130° is in good accord with the numerical predictions by Mulholland, Bohren and Fuller (1994) for larger fractal agglomerates composed of above 100 sub-units with random orientation. In particular, they reported the numerical simulation of an aggregate composed by 165 spheres with $m = 1.7 + i0.7$ and size parameter $x_P = 0.25$ ($x_P \equiv \pi a_P/\lambda$) and obtained a peak situated at varying angle (between 110 and 130°) depending on the choice of the approximation (CEMD, coupled electric and magnetic dipole; CED, coupled electric dipole) for the multipole expansion of the scattering by a sphere in the Mie series.

Fig. 4 shows an example (16 mm HAB) of normalised scattering pattern $I^A_{VV}(q)/I^A_{VV}(0)$ for cold ethylene flow rate of 11 cm^3 s^{-1}. Apparent flame length is about 17 cm. As a general trend, we can observe that the fractal dimension D^*_F is larger in the case of smaller cold gas flow rates at parity of axial co-ordinate. For instance, at 16 mm HAB is $D^*_F = 1.43 \pm 0.10$ and 1.22 ± 0.10 in the cases of 7 and 11 cm^3 s^{-1}, respectively. This can be physically explained from the fact that at lower gas flow velocity both primary particles and partially grown clusters mix and stick together and the combination of cluster–cluster aggregation with the monomer–cluster aggregation leads to an increase of the exponent D^*_F. Vice versa, for larger flow rates only clusters with the same history (age) meet and stick together and, consequently, the expected D^*_F is lower. Similar results were reported by Kütz and Schmidt-Ott (1993). Some deviation from the power-law regime is observed at higher q-values about 18 μm^{-1}. This can be commented reporting two arguments. First, at larger scattering angles (about 150–160°) the measurement volume is significantly larger that at 90°, owing to the fact that it scales with a factor $1/\sin\theta$, where θ is the scattering angles. Thus, polydispersion in the number of primary particle per aggregates can result in some deviation from a single power law. Second, at the decrease of q the scale of inspection tends to the so-called Porod's regime ($q \approx a_P^{-1}$), where spatial correlation within the fractal cluster are sensed on the scale dictated by the primary size. Fig. 5 shows the same analysis performed on the measurements obtained at 30 mm HAB. The values obtained for fractal dimension and gyration radius are 1.70 and 163 nm,

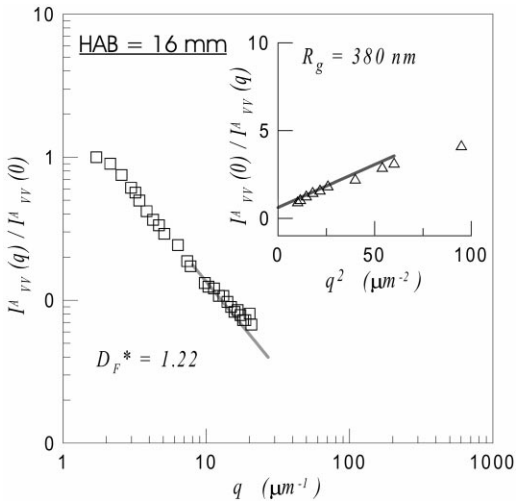

Fig. 4. Effective fractal dimension D_F^* (main graph) and gyration radius R_g (inset) as inferred by the scattering measurements at HAB = 16 mm. Same flame of Fig. 3.

respectively. As a matter of fact, a larger fractal dimension reflects a larger point mass density within fractal aggregates. In fact, for mass fractals the density inside a spherical surface with radius r and with centre at a point in the mass fractal centre is $\rho \propto r^{D_F^* - d}$, where d is the Euclidean dimension (see, for instance, Schmidt, 1991). Thus, the apparent compactness of the clusters is significantly higher at larger residence times. The outer dimension R_f of fractal aggregates is reported (Rogak, Flagan, & Nguyen, 1993) to be related to R_g by the equation $R_f = R_g\sqrt{(D_f^* + 1)/D_f^*}$. At the same HAB = 30 mm (Fig. 5) the onset of Porod's regime is observed to occur at $q \approx 20\ \mu m^{-1}$. In the same figure also some fluctuations in the measured scattered intensity can be observed. This could be derived from the turbulent mixing that occurs within the flame between gas fuel and ambient air. It is in principle possible to obtain a more stable flame by an external air or nitrogen flux co-annular with respect to the flame, but this trick is not used to avoid possible influence on the aggregate formation process. To get rid of these unwanted fluctuations, the scattering measurements considered in this work are thus limited to explore HABs within about one fourth (~ 4 cm) of the overall flame length (~ 17 cm) where flame is more stable.

In Fig. 6, the experimental values of fractal dimension are reported against those of radius of gyration at a number of 7 different heights above the burner. Measurement points in the plot are connected to a spline fit. About the significance of the fractal dimension determined at heights of 4–8 mm, it is worthwhile to recognise that a fractal dimension 2.6 reported at HAB = 4 mm represents the case of not yet aggregated primary particles that pass through the measurement volume (Mikhailov & Vlasenko, 1995). The agglomeration process starts significantly at about 8 mm HAB in correspondence with the strengthening of forward scattering with respect to the flat I^A_{VV} angular patterns observed at lower axial co-ordinates.

At 10–16 mm HABs a fractal dimension D_F^* in the range 1.2–1.35 is inferred, which corresponds to the formation of chain-like clusters. This kind of elongated clusters continue to develop in their length at larger HABs, essentially at parity of fractal dimension (D_F^* about 1.3), until an aggregate

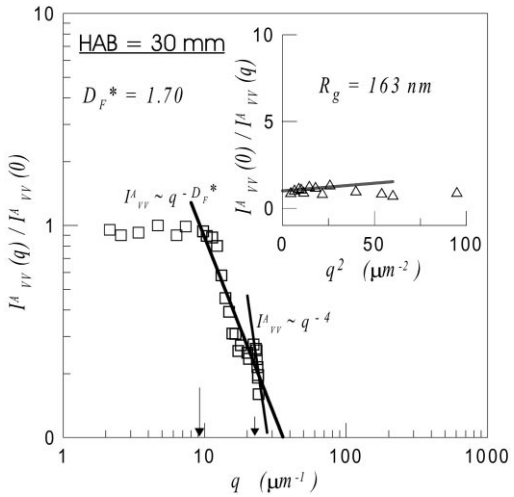

Fig. 5. Same for Fig. 4 but at HAB = 30 mm. Thick and thin lines are interpolation of the experimental data in fractal power law and Porod's regimes, respectively. The longer and shorter arrows near the abscissa axis indicate, respectively, the values $q \approx \xi^{-1}$ and $q \approx a_P^{-1}$ that are the lower and upper limits for the validity of power law regime.

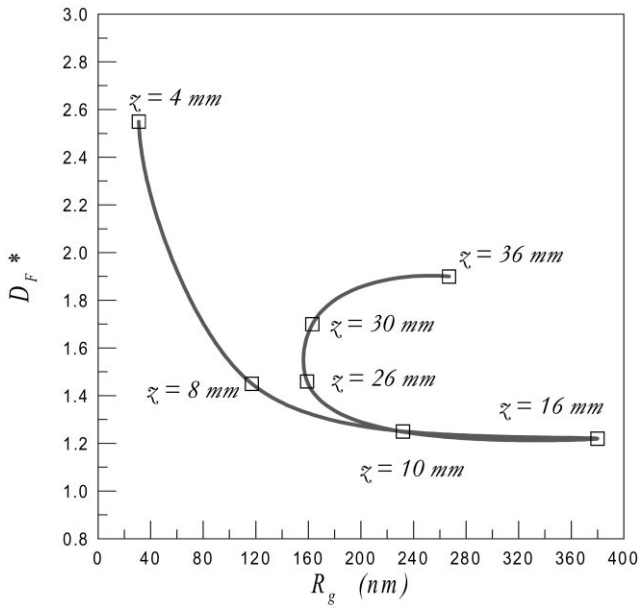

Fig. 6. Plot of D_F^* vs. R_g as inferred at different HABs. Same flame conditions of Fig. 3.

size of about 500 nm ($R_g = 380 \pm 24$ nm) is observed at HAB = 16 mm. Thereafter, for axial co-ordinates larger than 16 mm, a spatial reorganisation of the agglomerate structure occurs. This is evidenced, between 16 and 26 mm HABs, by the fact that a nearly constant D_F^* is observed, whereas R_g reduces from about 380 nm to 170 nm. At HABs larger than 26 mm, D_F^* evolves from

1.3–1.4, which characterises branched chain-like morphology, to larger values ($D_F^* \approx 1.7$) that are characteristics of extended fractal assemblies. In the final stages of the process (HABs larger than 30 mm) an agglomeration process that involves sticking of sub-clusters leads to the formation of agglomerates with D_F^* about 1.8 ± 0.10, which is the value expected from the simulations for diffusion-limited cluster–cluster agglomeration (Lin et al., 1990).

The qualitative behaviour here shown by R_g and D_f^* at different HABs is in surprising accord with the results reported very recently by Xing, Köylü and Rosner (1999) for inorganic alumina (Al_2O_3) aggregates of nanoparticles produced in a quite different combustion facility. In particular, those authors used a laminar counterflow nonpremixed methane flame to synthesise aluminium oxide particles by the reaction of water vapour from overfire region of flame with evaporated trimethylaluminium (TMA) containing 3% $AlH(CH_3)_2$. Nevertheless, in that configuration, alumina nanoparticles do form fractal aggregates before they meet the high-temperature (2000 K) counterflow flame region. Owing to this fact, the restructuring process by fractal aggregates is therein justified by a sintering mechanism, probably occurring.

By contrast, in our case, aggregate sintering was not observed in the SEM samples probed at the considered low HABs ($< 0.25 L_{flame}$). Thus, the self-compacting of aggregate structure seems to be caused more probably by physical mechanisms, such as some elastic–mechanical strain effects on aggregate surface, or thermal settling of the aggregate structure or charge localisation at agglomerate tips. In this regard, the last conjecture is the object of current research (Onischuk et al., 2000a, b). With concern to the possibility of thermal settlement, it should be reminded that, at the increasing of the residence times, soot particles undergo a de-hydrogenation process (Haynes & Wagner, 1981; Kennedy, 1997). Several studies exist in the literature of aerosol particles, such as in the case of hydrogenated amorphous silicon (Allan & Joannopoulos, 1984; Onischuk et al., 1997) that report about the correlation between hydrogen concentration in particles and the degree of order in amorphous solid-state network. The amount of the ratio hydrogen to carbon (H/C) is found by experiments to yield significant influence on the optical properties of soot (Habib & Vervisch, 1988). About the microstructure of soot, evidence has been recently reported for soot aggregates that the agglomeration mechanism occurs contemporarily to surface growth (Ishiguro, Takatori, & Akihama, 1997) and on different scale lengths (di Stasio, 2000b). As a matter of fact, the restructuring mechanism here observed is relative to the transformation of elongated aggregate shapes to more compact morphologies. At this regard, the two limiting cases of cylindrically and spherically shaped clusters are characterised by completely different radiative heat transmission. Thus, for instance, in the case of small soot particles (size parameter < 0.1) with random orientation and at parity of volume fraction, the spectral emissivity of cylindrical particles is at visible wavelengths much lower (from 5 to 30% depending on the volume fraction) with respect to the spheroid shape (Lee & Tien, 1983; Charalampopoulos & Hahn, 1989; di Stasio & Massoli, 1994). Thus, an enhancement of the local temperature of cluster surface in the case of cylindrically shaped aggregates is somehow expected. As a consequence of this, some restructuring could occur in cylindrical aggregates, in particular owing to the supplementary oxidation of primary particles that constitute the skeleton of the aggregates. In particular, the local temperature enhancement of soot surface could produce in some hypotheses, related to the O_2 contents of particles (Neoh, Howard, & Sarofim, 1984; di Stasio, 2000b) the scavenging of the particle from their inside, namely a supplementary oxidation could occur inside the pores of soot. This effect could be put into relationship with the structural bending of the aggregates that collapse into more compact

morphologies. When progressive dehydrogenation of inner nuclei of primary nanoparticles verifies (Ishiguro et al., 1997) as consequence of the high-temperature oxidative process, it is reasonable to expect the occurring of cracking or fractures in the graphitic planes linking adjacent spherules. This explanation is coherent with some results reported for diffusion flames by some other authors (Furutami, Tsuge, & Goto, 1992) about the correlation existing between the soot H/C ratio, which is progressively decreasing during oxidation process, and the decreasing equivalent diameter of soot particles. It should also be commented that the decreasing of the external size of soot aggregates while fractal dimension is practically constant, here observed at HABs between 10 and 26 mm, could be represented in terms of the variation with opposite trends of smaller and larger scaling cut-off lengths, a_P and ξ, respectively. During the central phase of the compacting process a_P and ξ should tend to each other, while keeping constant the exponent $D_F^* \approx 1.3$ of the power-law density correlation within the fractal aggregates. This is the same arguments reported by Sempéré, Bourret, Woignier, Phalippou and Jullien (1993) to explain the gradual reduction of the extension of fractal regime during the sintering of silica aerogels at different temperatures observed by small angle neutron scattering (SANS).

From the results shown in Fig. 6 in the cases HAB = 10–16 mm, it comes out the essential utility of some other scattering diagnostic to distinguish between the cases of nanoparticle aggregates with very similar fractal dimension. At this aim, systematic measurements of the depolarisation ratio were performed. Fig. 7 reports the experimental data of the vertical depolarisation ratio $\rho_V \equiv I_{HV}/I_{VV}$ at 90° plotted against the height-above-burner HAB. Form the direct comparison with Fig. 6 it can be directly observed that agglomerates with practically constant D_F^* produce different ρ_V. In particular, ρ_V sharply increases at the onset of the agglomeration process when

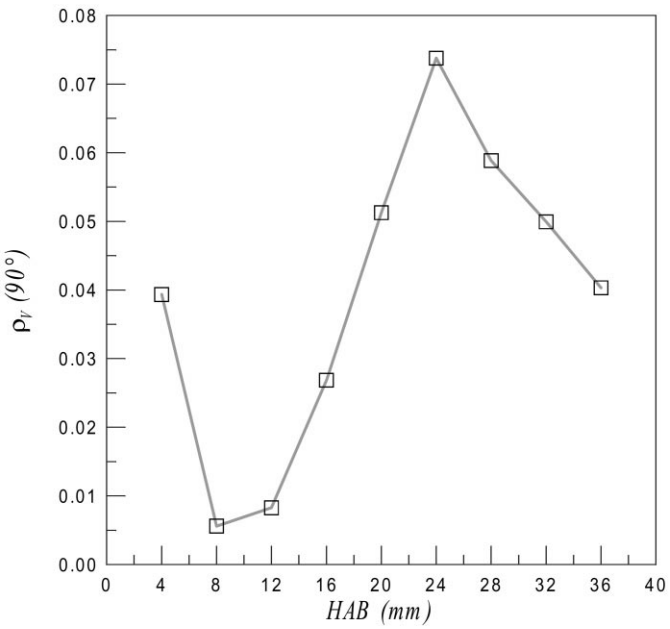

Fig. 7. Vertical depolarisation ratio at $\theta = 90°$ against HAB for the same flame conditions of Fig. 3.

shorter chain-like aggregates are formed (HAB = 8–26 mm). For a nearly constant fractal dimension $D_F^* \approx 1.3$–1.4, observed for HABs between 10 and 26 mm, the depolarisation ratio ρ_V changes within these extreme cases of a factor about 6. Thereafter, at the onset of the restructuring process (HAB > 26 mm), ρ_V is observed to slightly decrease in correspondence the formation of aggregates with higher fractal dimension. From a theoretical point of view, the information about depolarised scattered light is expected to be complementary with respect to the fractal dimension, which is worked out from the measurements of co-polarised scattered light I_{VV}. In fact, it can be demonstrated that the depolarised light I_{HV} (Chen, Weakliem, Gelbart, & Meakin, 1987) is sensitive to the short-range interactions (nearest-neighbour distribution) which are described in terms of the contributions of the scattered light which bounces at least *twice* within the cluster before being collected by the detector. Vice versa, that portion of laser light which induces electrical polarisation inside *one* particle in the agglomerate before its arrival on detector (that is here considered to infer fractal dimension and radius of gyration), results strictly polarised with the same polarisation state of the incident light (Dimon et al., 1986). Thus, the long-range spatial correlation (Chen et al., 1987) within the fractal aggregates cannot be described in terms of depolarised light, which in turn, is strictly depending on the near surrounding neighbours of the single primary particle within an aggregate.

5. Conclusions

This paper reports and discusses the evidence, obtained by static light scattering experiments of a *spatial restructuring* process occurring for nanoparticle aggregates of different age within a diffusion flame along the flame axis. In particular, at lower residence times (lower HABs, $\sim$10 mm), soot primary spherules in the scattering volume do agglomerate as branched elongated chains ($D_F^* \approx 1.2$–1.3). Thereafter, at longer residence times (higher HABs, $\sim$30 mm), soot aggregates collapse on themselves by the generation of more compact clusters with larger fractal dimension ($D_F^* \approx 1.7$–1.9). Such a compacting mechanism is observed to start at a fractal dimension $D_F^* \approx 1.3$ and radius of gyration $R_g \approx 380$ nm. Explanation of the experimental results is given in terms of a possible local temperature enhancement at the surface of the chain-like clusters with a consequent supplementary oxidation occurring within the pores of primary particle. Thus, the eventual breaking of graphitic layers at contact loci between primary particles it is thought to be responsible for the aggregate restructuring with the formation inside the flame of more compact structures. The experimental results here reported do not rely on any assumption about the soot refractive index $m = n + ik$. The restructuring mechanism is observed to occur at larger gaseous fuel flow rates (≈ 11 cm^3 s^{-1}) but not at lower flow-rates (≈ 7 cm^3 s^{-1}), at which aggregates with practically the same fractal dimension (D_F^* about 1.4) are found to grow up.

References

Allan, D., & Joannopoulos, J. D. (1984). Theory of electronic structure. In J. D. Joannopoulous & G. Lucovsky (Ed.), *The Physics of hydrogenated amorphous silicon (II)*. Berlin: Springer.

Asnaghi, D., Carpineti, M., Giglio, M., & Sozzi, M. (1992). *Physical Review*, *A 45*, 1018.

Bohren, C. F., & Huffman, D. R. (1983). *Absorption and scattering of light by small particles*. New York: Wiley.
Bunde, A., & Havlin, S. (1994). In A. Bunde, & & S. Havlin (Eds.), *Fractals in Science, (p. 16)*. Berlin: Springer.
Bunde, A., & Havlin, S. (1996). In A. Bunde, & & S. Havlin (Eds.), *Fractals and disordered systems, (pp. 59–113)*. Berlin: Springer.
Burtscher, H., Leonardi, A., Steiner, D., Baltensperger, U., & Weber, A. (1993). *Water, Air, and Soil Pollution*, *68*, 137.
Charalampopoulos, T. T., & Hahn, D. W. (1989). *Journal of Quantitative Spectroscopy and Radiative Transfer*, *42*, 219.
Chen, G. (1996). *Journal of Heat Transfer*, *118*, 539.
Chen, Z.-Y., Weakliem, P., Gelbart, W. M., & Meakin, P. (1987). *Physical Review Letters*, *58*, 1996.
Dimon, P., Sinha, S. K., Weitz, D. A., Safinya, C. R., Smith, G. S., Varady, V. A., & Lindsay, H. M. (1986). *Physical Review Letters*, *57*, 595.
di Stasio, S. (2000a). *Applied Physics B 70*, 635.
di Stasio, S. (2000b). *Carbon 39*, 109–118.
di Stasio, S., & Massoli, P. (1994). *Measurement Science Technology*, *5*, 1453.
di Stasio, S., & Massoli, P. (1997). *Combustion Science and Technology*, *124*, 219.
di Stasio, S., & Massoli, P. (1998). *Particle Particle Systems Characters*, *15*, 90.
Dobbins, R. A., & Megaridis, C. M. (1991). *Applied Optics*, *30*, 4747.
Dobbins, R. A., Mulholland, G. W., & Bryner, N. P. (1994). *Atmospheric Environment*, *28*, 889.
Dobbins, R. A., Santoro, R. J., & Semerjian, H. G. (1990). *XXIII symposium (international) on combustion, (pp. 1525–1532)*. Pittsburgh: The Combustion Institute.
Faeth, G. M., & Köylü, Ü. Ö. (1995). *Combustion Science and Technology*, *108*, 207.
Feng, S. (1985). *Physical Review*, *B, 32*, 5793.
Freltoft, T., Kjems, K. K., & Sinha, S. (1986). *Physical Review*, *B, 33*, 269.
Friedlander, S. K., Jang, H. D., & Ryu, K. H. (1998). *Applied Physics Letters*, *72*, 173.
Furutami, H., Tsuge, S., & Goto, S. (1992). *SAE paper 920689* Soc. Automotive Eng. Inc., Warrendale PA, (pp. 161–166).
Gangopadhyay, S., Elminyawi, I., & Sorensen, C. M. (1991). *Applied Optics*, *30*, 4859.
Habib, Z. G., & Vervisch, P. (1988). *Combustion Science and Technology*, *59*, 261.
Haw, M. D., Poon, W. C. K., & Pusey, P. N. (1997). *Physical Review*, *E, 56*, 1918.
Haynes, B. S., & Wagner, H. G. G. (1981). *Progress in Energy and Combustion Science*, *7*, 229.
Howard, J. B. (1969). *XII symposium (international) on combustion, (pp. 877–887)*. Pittsburgh: The Combustion Institute.
Hurd, A. J., & Flower, W. L. (1988). *Journal of Colloid Interface Science*, *122*, 178.
Ishiguro, T., Takatori, Y., & Akihama, K. (1997). *Combustion and Flame*, *108*, 231.
Kasper, G. (1982). *Aerosol Science and Technology*, *1*, 187.
Kaye, G. W. C., & Laby, T. H. (1966). *Physical and Chemical Constants, (p. 40)*. London: Longmans, Green & Co Ltd.
Kennedy, I. M. (1997). *Progress in Energy and Combustion Science*, *23*, 95.
Kjems, J. K. (1996). In A. Bunde, & & S. Havlin (Eds.), *Fractals and disordered systems, (pp. 303–337)*. Berlin,: Springer.
Köylü, Ü. Ö. (1996). *Combustion and Flame*, *109*, 488.
Köylü, Ü. Ö., Xing, Y., & Rosner, D. E. (1995). *Langmuir*, *11*, 4848.
Kütz, S., & Schmidt-Ott, A. (1993). *Journal of Aerosol Science*, *24* (Suppl. 1), s553.
Lee, S. C., & Tien, C. L. (1983). *Journal of Quantitative Spectroscopy and Radiative Transfer*, *29*, 259.
Lin, M. Y., Lindsay, H. M., Weitz, D. A., Klein, R., Ball, R. C., & Meakin, P. (1990). *Journal of Physics and Condensed Matter*, *2*, 3093.
Malcai, O., Lidar, D. A., Biham, O., & Avnir, D. (1997). *Physical Review*, *E, 56*, 2817.
Martin, J. E., & Hurd, A. J. (1987). *Journal of Applied Crystallography*, *20*, 61.
Megaridis, C. M., & Dobbins, R. A. (1989). *Combustion Science and Technology*, *66*, 1.
Mikhailov, E. F., & Vlasenko, S. S. (1995). *Physics-Uspekhi*, *38*, 253.
Mulholland, G. W., Bohren, C. F., & Fuller, K. A. (1994). *Langmuir*, *10*, 2533.
Neoh, K. G., Howard, J. B., & Sarofim, A. F. (1984). *XX symposium (international) on combustion, (pp. 951–957)*. Pittsburgh, PA: The Combustion Institute.
Nyeki, S., & Colbeck, I. (1995). *Aerosol Science and Technology*, *23*, 109.
Oh, C., & Sorensen, C. M. (1997). *Journal of Aerosol Science*, *28*, 973.

Onischuk, A.A., di Stasio, S., Karasev, V.V., Strunin, V.P., Baklanov, A.M., & Panfilov, V.N. (2000a). *Journal of Physical Chemistry A*, 104, In Press (Web Release: Sept. 6).
Onischuk, A.A., di Stasio, S., Strunin, V.P., Karasev, V.V., Baklanov, A.M., & Panfilov, V.N. (2000b). Journal of Aerosol Science, 31 (Supp 1) S950.
Onischuk, A. A., Strunin, V. P., Samoilova, R. I., Nosov, A. V., Ushakova, M. A., & Panfilov, V. V. (1997). *Journal of Aerosol Science*, *28*, 1425.
Rogak, S. N., Baltensperger, U., & Flagan, R. C. (1991). *Aerosol Science and Technology*, *14*, 447.
Rogak, S. N., Flagan, R. C., & Nguyen, H. V. (1993). *Aerosol Science and Technology*, *18*, 25.
Santoro, R. J., Smerjian, H. G., & Dobbins, R. A. (1983). *Combustion and Flame*, *51*, 203.
Schmidt, P. W. (1991). *Journal of Applied Crystallography*, *24*, 414.
Schmidt-Ott, A. (1988a). *Applied Physics Letters*, *52*, 954.
Schmidt-Ott, A. (1988b). *Journal of Aerosol Science*, *19*, 553.
Schmidt-Ott, A., Baltensperger, U., Gäggeler, H. W., & Jost, D. T. (1990). *Journal of Aerosol Science*, *21*, 711.
Sempéré, R., Bourret, D., Woignier, T., Phalippou, J., & Jullien, R. (1993). *Physical Review Letters*, *71*, 3307.
Sorensen, C. M., Cai, J., & Lu, N. (1992). *Applied Optics*, *31*, 6547.
Sorensen, C. M., & Feke, G. D. (1996). *Aerosol Science and Technology*, *25*, 328.
Sorensen, C. M., Lu, N., & Cai, J. (1995). *Journal of Colloid and Interface Science*, *174*, 456.
Thouy, R., & Jullien, R. (1996). *Journal of Physics I France*, *6*, 1365.
Weber, A. P., & Friedlander, S. K. (1997a). *Journal of Aerosol Science*, *28*, s765.
Weber, A. P., & Friedlander, S. K. (1997b). *Journal of Aerosol Science*, *28*, 179.
Webman, I., & Grest, G. S. (1985). *Physical Review*, *B, 31*, 1689.
Wersborg, B. L., Howard, J. B., & Williams, G. C. (1973). *XIV symposium (international) on combustion, (pp. 929–940)*. Pittsburgh, PA: The Combustion Institute.
Xing, Y., Köylü, Ü. O., & Rosner, D. E. (1999). *Applied Optics*, *38*, 2686.